Multiobjective optimization of dimension and position of elliptical crush initiator on crashworthiness performance of square tube using response surface methodology

M. Hafid, Jos Istiyanto* and Nasruddin Nasruddin

Department of Mechanical Engineering, Universitas Indonesia, Depok, Indonesia

In this study, the crashworthiness performance of a thin-walled square steel-tube structure with an elliptical crush initiator under impact loading was investigated. The effect of the height, width, and distance of the crush initiator from the top of the tube on the crashworthiness performance was analyzed using several numerical simulations using ABAQUS Explicit. The response surface methodology was used to predict the crashworthiness performance indices, and optimization was performed to determine the optimal dimensions and position of the crush initiator. The optimization was aimed at minimizing the peak force (PF) while maximizing the mean crushing force (MCF), crush force efficiency (CFE), and specific energy absorption (SEA). The result was an elliptical crush initiator with a height of 15 mm, width of 24.784 mm, and distance of 15.08 mm. Validation was performed to verify these results. The optimal crush initiator effect resulted in a 10.12% decrease in the peak force, 13.67% increase in the crush force efficiency, and 2.23% increase in the mean crushing force. However, a slight decrease of 0.82% in specific energy absorption was observed.

1 Introduction

Thin-walled tubes, which are used to absorb energy during collisions, have been extensively investigated in the automotive industry. Various researchers have used experiments, numerical simulations, and theoretical analyses to reveal their energy absorption capabilities. To minimize passenger injury, various researchers focused their studies on several parameters, such as the peak force (PF), mean crushing force (MCF), crush force efficiency (CFE), and specific energy absorption (SEA). Numerous studies have been conducted to determine the effects of various crush initiators, including cut-out and foam packing. These studies revealed the potential of decreasing PF and increasing SEA.

Some studies have investigated the use of cut-outs as crush initiators to reduce the PF while maintaining the MCF. The geometry and position of the cross-section and the crush initiator increase the CFE of tube structures. Nghia et al. (2013) developed an analytical model for a square thin-walled aluminum tube with a circular cut-out as the crush initiator,

which effectively decreased the PF in the first fold while maintaining a similar MCF. Subramaniyan et al. (2014) found that the quantity of circular cut-outs contributed to decreasing the PF in circular and square tubes. Other studies examined the impact of crush initiator placement, such as drilling holes (Estrada et al., 2019) and multiple holes (Malawat et al., 2019; Dionisius et al., 2022) in square steel tubes, leading to improved crashworthiness performance. Researchers have examined the use of V-notch, groove (Balaji and Annamalai, 2017), and tapered (Asanjarani et al., 2018) shapes as effective crush initiators, reducing the initial force spikes without compromising the total energy absorption. Hexagonal (Rogala et al., 2021b) and elliptical (Cheng et al., 2006) cut-outs in square aluminum tubes have been analyzed, revealing their significant influence on decreasing the PF. The position and width-to-height ratio of the cut-out are critical factors that influence PF reduction.

For inflexible foam applications, various studies have aimed to enhance the energy absorption capacity while maintaining the PF in tubular structures. For instance, Rezvani and Jahan (2015) investigated a circular aluminum tube reinforced with an annular ring and rigid polyurethane foam, which showed improved energy absorption and CFE using a specific design. Razazan et al. (2018) developed a shock absorber with a crush initiator on a rectangular aluminum tube filled with rigid polyurethane foam, which exhibited a higher energy absorption capacity than partially filled structures. Studies on thin-walled square aluminum tubes with foam and various crush initiators have shown that structures with four holes at the corners (Li et al., 2019) demonstrate the best crashworthiness performance. Rogala et al. (2021a) analyzed the effect of impact load on the dimple depth and diameter by incorporating aluminum foam to improve the CFE without increasing the initial PF, leading to an increased MCF.

The cut-out position and width of the crush initiator parameter influence the PF more significantly than the height (Huang et al., 2010; Rogala et al., 2021b) under impact loads. However, studies addressing the crashworthiness performance, dimension optimization, and optimal positioning of a cut-out in an energy-absorbing structure are rare. This study addresses this problem by introducing an elliptical cutout model in which various heights, widths, and distances from the top end are optimized. The elliptical shape was selected owing to its composition of two circular axes, which are easier to manufacture than a hexagonal shape, but slightly more intricate than a simple circular hole.

This study is primarily aimed at investigating the relationship between the cut-out parameters and the crashworthiness performance of a thin-walled square steel tube. Moreover, this study focused on identifying the most significant parameters influencing crashworthiness and clarifying the interactions between these parameters. Subsequently, optimization was conducted to determine suitable geometric parameters capable of enhancing the CFE while preserving the SEA of the square-tube structure.

2 Materials and methods

2.1 Crashworthiness performance indicators

The capacity of a structure to absorb the energy generated from an impact or crash is called the energy absorption in crash testing. Several crash tests involve subjecting a material or structure to collision with an object at a predetermined velocity, and the absorbed energy is subsequently determined (Guler et al., 2010; Sun et al., 2017). This aspect is of the utmost importance in designing structures or vehicles to minimize human injuries and vehicle damage. Eq. 1 is the formula for calculating the energy absorption (EA):

$$EA(\delta) = \int_0^\delta F(\delta)d\delta \qquad (1)$$

where F is the crushing force, and δ is the displacement. Therefore, the SEA is calculated using Eq. 2:

$$SEA(\delta) = \frac{EA(\delta)}{m} = \frac{\int_0^\delta F(\delta)d\delta}{m} \qquad (2)$$

where m is the mass of the specimen. Crash test data can be used to calculate the MCF. This value is obtained using Eq. 3:

$$MCF = \frac{\sum_{i=1}^N F_i}{N} \qquad (3)$$

where N is the number of data points, and i is the index for the i th data point. The CFE is calculated using Eq. 4.

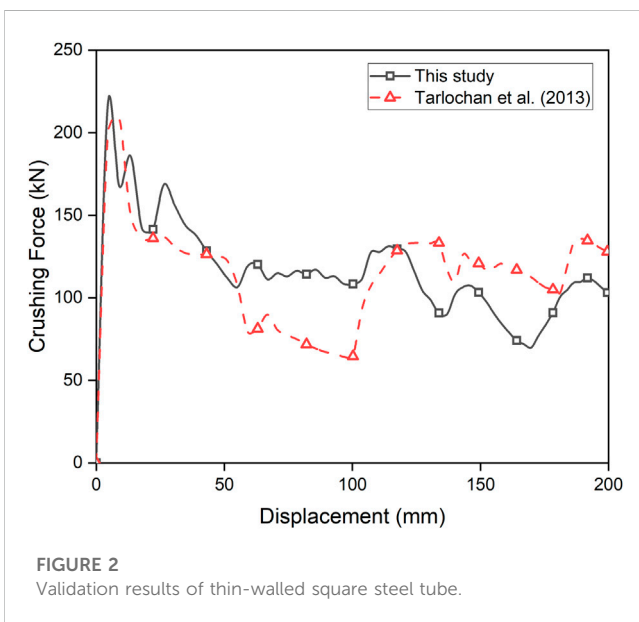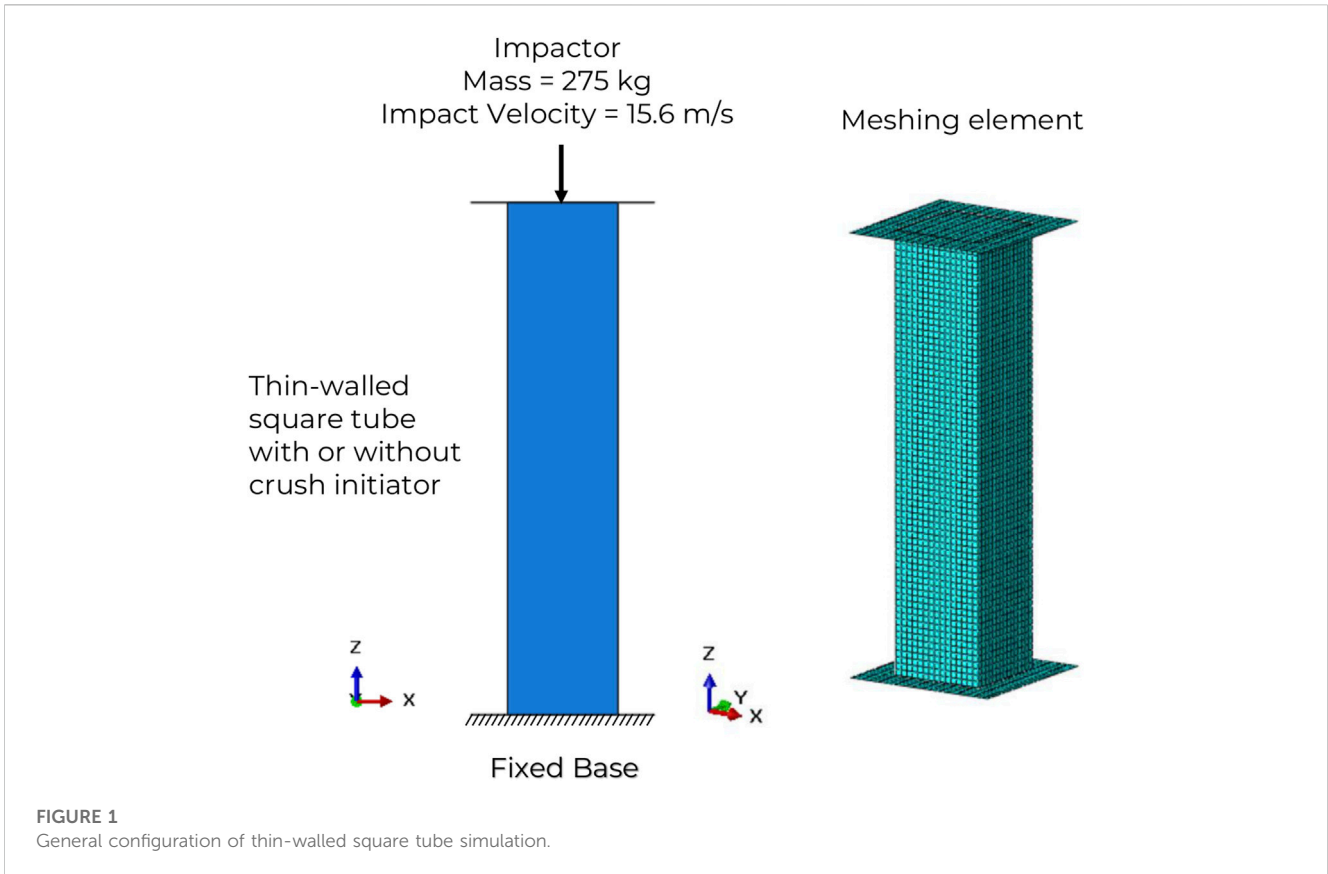$$CFE = \frac{MCF}{PF} \qquad (4)$$

The PF is obtained from the force–displacement graph. This represents the maximum force experienced during collision, which typically occurs at the beginning, when the highest impact velocity is reached. The PF measurement plays a crucial role in evaluating the EA capability of a material or structure and in predicting potential damage.

2.2 Square tube validation

Validation was conducted to ensure the accuracy, reliability, and suitability of various simulation results serving as information for researchers to make decisions. It was achieved by comparing the simulation results with the data obtained from other trusted sources. A validation simulation typically involves a top–down arrangement consisting of an impactor, a thin-walled square tube, and a fixed base. Figure 1 illustrates the meshing and overall arrangement of a rigid shell plane with several 5 mm elements used in the energy-absorbing structure.

The cross-sectional measurements of the square tube were derived from the typical average perimeter of the tubes used in sedans (Tarlochan et al., 2013). The simulated tube had a 300 mm perimeter, 350 mm length, 1.7 kg mass, 75 mm × 75 mm major dimension, and 2 mm thickness. The impact simulation results are depicted by a curve showing the crushing force *versus* displacement (Figure 2). An insignificant difference exists between the conducted simulation and reference simulation results. In this study, the significance of the differences in the calculated values of the generated curves was determined.

Based on the data processing, it was found that the most significant difference in the crashworthiness indicator values between the simulation results and the reference was 3.9% for the PF, as listed in Table 1. This difference may not be significant; therefore, we may further investigate various optimization processes for tube structures incorporating the crush initiator.

FIGURE 1
General configuration of thin-walled square tube simulation.

FIGURE 2
Validation results of thin-walled square steel tube.

TABLE 1 Errors between conducted results of simulations and reference.

Reference	PF (kN)	MCF (kN)	CFE	SEA (kJ/kg)
This study	217.03	112.78	0.52	14.01
Tarlochan et al. (2013)	208.92	115.78	0.53	13.66
Error	+3.9%	−2.6%	−1.9%	+2.6%

$$MCF = M_0\left[\left\{1+\left(\frac{0.41V}{c_t D}\right)^{1/p}\right\}\left\{46.16\left(\frac{c_t}{h}\right)^{1/3}+2.14\left(\frac{c_t}{h}\right)^{2/3}+1.30\right\}\right]$$

$$(5)$$

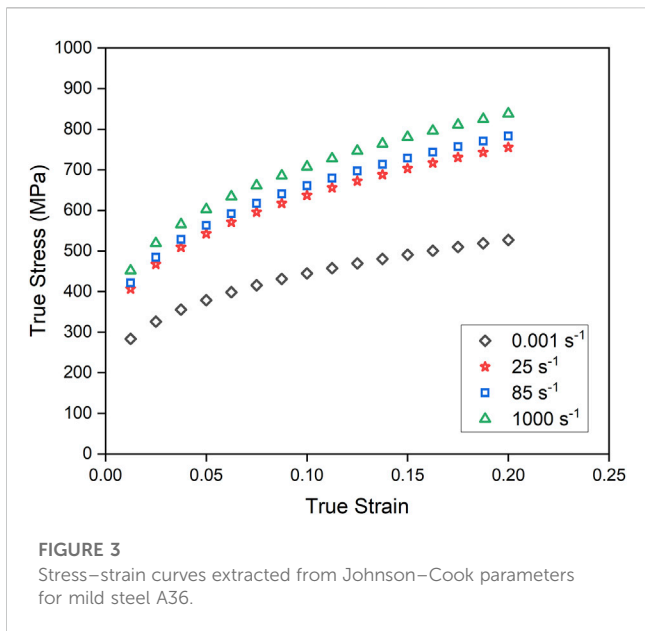$$2H = 1.66c_t^{2/3}h^{1/3} \tag{6}$$

where $M_0 = \sigma_0 h^2/4$, σ_0 is the flow stress, h is the thickness of the tube, V is the velocity of the impactor, c_t is the length of a side of the square tube, $D = 6844$ s^{-1}, $p = 3.91$, and H is half of the initial distance of the wavelength. Therefore, the simulation results can be cross-referenced with analytical calculations to validate the progressive buckling behavior of a thin-walled square tube obtained *via* numerical simulations. Eq. 7 provides the strain rate (Abramowicz and Jones, 1984) resulting from the dynamic crushing of a square tube undergoing an asymmetric mixed collapse mode B:

$$\dot{\varepsilon} = 0.41V/c_t \tag{7}$$

where $\dot{\varepsilon}$ is the strain rate.

For simplicity, the analytically calculated values of the MCF and first folding wavelength were 113.02 kN and 37.2 mm, respectively.

The authors observed the occurrence of the asymmetric mixed collapse mode B in the current problem. This mode was determined using the analytical equations derived by Abramowicz and Jones (1984), which provide the MCF values for a thin-walled square tube and the first-fold wavelength of the basic collapse element, expressed by Eqs 5, 6, respectively:

FIGURE 3
Stress−strain curves extracted from Johnson−Cook parameters for mild steel A36.

The flow stress was determined using the Johnson–Cook constitutive model for mild steel A36 material (Lacy, 2010), as shown in Figure 3. The material exhibited high sensitivity to strain rate, with increased strain rates resulting in increased flow stress. From Eq. 7, the strain rate generated during the drop impact scenario was approximately 85 s^{-1}, yielding a corresponding flow stress of 421.24 MPa. The initial distance measured between the upper point (P_u) and lower point (P_l) of the first folding wavelength was 40 mm, as shown in Figure 4. The difference in the wavelength

of the first folding between the numerical results and the calculated values obtained using Eq. 6 was smaller than the meshing size of 5 mm. Therefore, the numerical results for the impact on the square tube in this study show satisfactory agreement with the analytical predictions.

2.3 Response surface methodology-based predictive model

The experimental design was used to examine the relationship between the experimental parameters and responses. Three parameters were selected as input variables, and their effects on the responses were observed using a face-centered central composite design (CCD). The three factors analyzed were the height, width, and distance between the center point of the crush initiator and the top of the tube, as shown in Figure 5, as well as the detailed geometry illustrated in Figure 6. An empirical correlation was established, based on the results of the experimental design, which were statistically analyzed using an RSM. RSM is a reliable analytical method that employs a second-order polynomial for investigating the effects of these input variables (Sahoo, 2011; Nagaraju et al., 2016; Deshwal et al., 2020). The analysis of variance (ANOVA) was employed to examine the significance of the model and input parameters by calculating the mean squared, degrees of freedom, and sum of the squared deviations for each input (Maqsood et al., 2022). A significance level of 5% was applied to determine the significant input values, and the p-value was used to assess the acceptance or rejection of the null hypothesis by the model. A lower p-value provides more significant evidence to reject the null hypothesis, indicating a more compelling indication that the
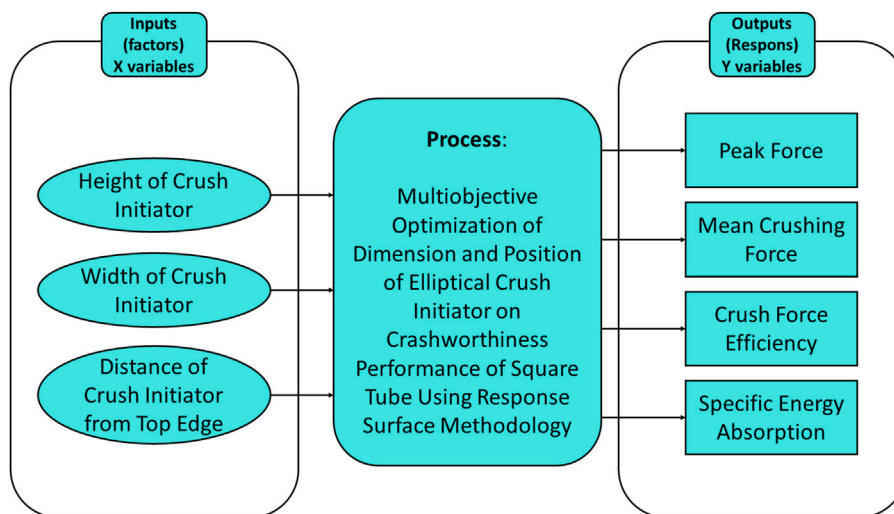

FIGURE 4
Numerical solution for upper and lower points of first folding wavelength.
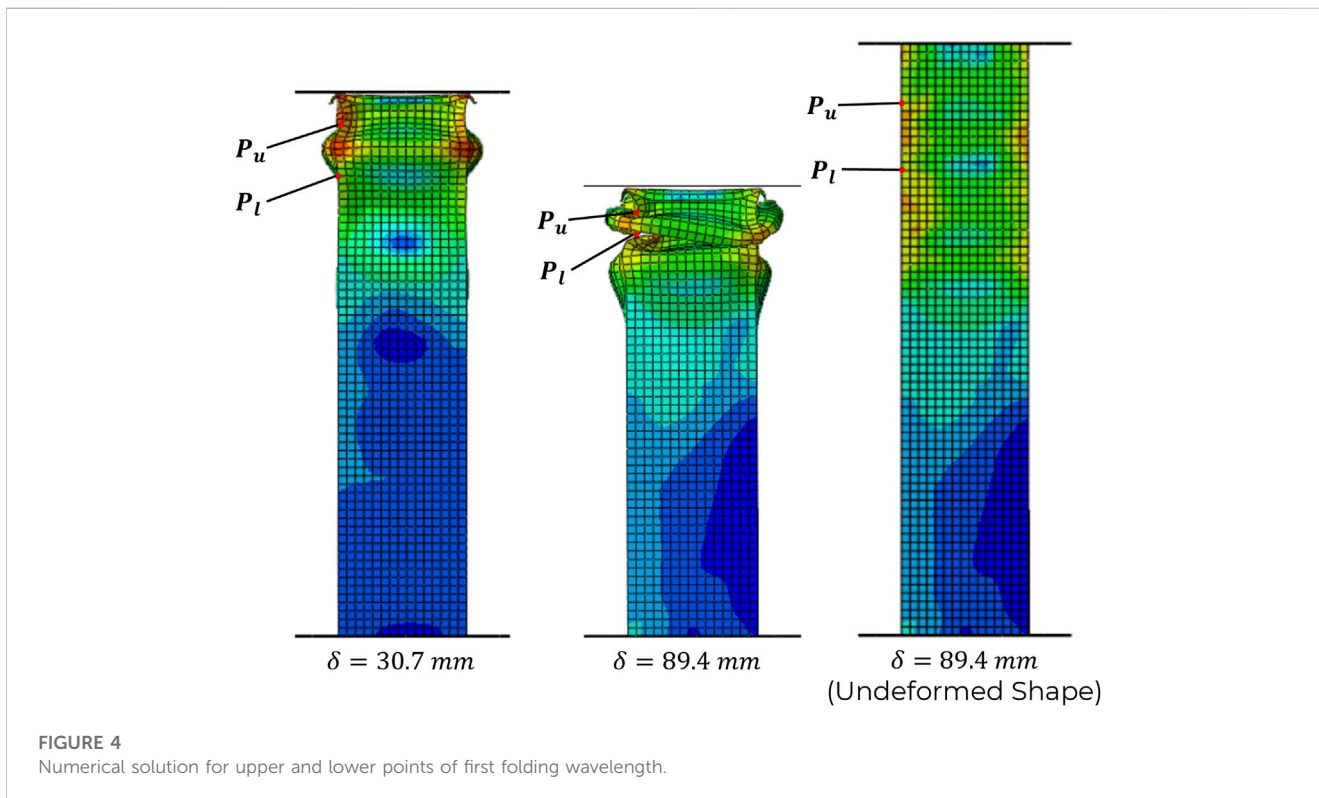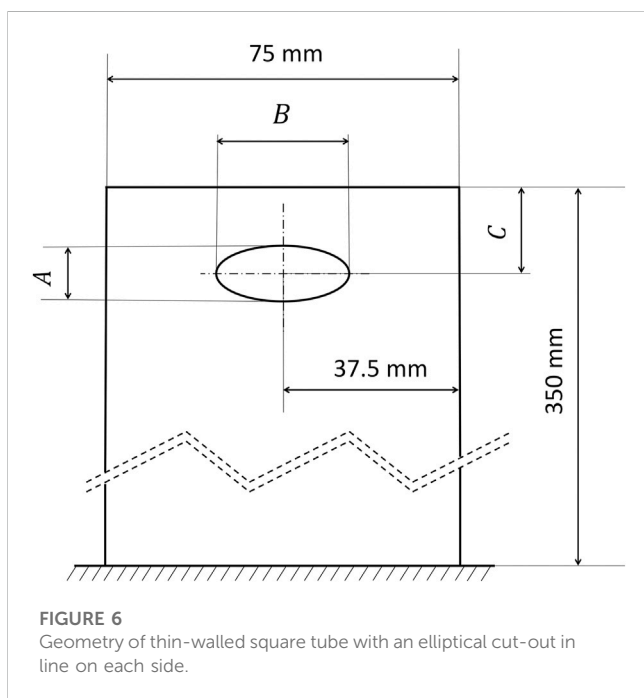
FIGURE 5
Design of experiment.

FIGURE 6
Geometry of thin-walled square tube with an elliptical cut-out in line on each side.

model is significant. The key aspect of the RSM is the derivation of various mathematical formulas that express the relationship between the response and input variables (Dadrasi et al., 2020). This relationship is expressed as a quadratic equation (Eq. 8):

$$R(A, B, C) = ¥_0 + \sum ¥_i A + \sum ¥_j B + \sum ¥_k C + \sum ¥_{ij} AB + \sum ¥_{ik} AC + \sum ¥_{jk} BC + \sum ¥_{ii} A^2 + \sum ¥_{jj} B^2 + \sum ¥_{kk} C^2$$

(8)

where R is the proposed expected response, $¥_0$ is the regression constant, $¥_i$, $¥_j$, and $¥_k$ are the linear coefficients, $¥_{ij}$, $¥_{ik}$, $¥_{jk}$ are the first-order interaction effects, $¥_{ii}$, $¥_{jj}$, and $¥_{kk}$ are the square terms of

each factor, and A, B, and C are the input or predictor variables. By generating a three-dimension surface plot based on the derived formula, the optimization process of a square tube structure with an elliptical crush initiator was enabled.

The low and high values of the height were 5 and 15 mm, respectively. The low and high values of the width were 10 and 35 mm, respectively, and those of the distance were 15 and 40 mm, respectively. A CCD with six center points suggests conducting 20 runs with varying input parameters for the geometry and position of the crush initiator in the square-tube structure. The response variables of interest are the PF, MCF, CFE, and SEA, as shown in Figure 5.

2.4 Square tube modeling with ellipse cut-out

After the validation was completed, the square tube structures with the optimized elliptical crush initiators were designed, based on Figure 1. The design of the elliptical crush initiator was based on three geometric parameters: height (A), width (B), and the center-to-center distance of the cut-out from the top end of the square tube (C). Impact tests were conducted at an impactor velocity of 15.6 m/s and a mass of 275 kg to evaluate the crashworthiness of the tube (Witteman, 1999; Tarlochan et al., 2013). Figure 6 depicts the geometry of a square tube with an elliptical cut-out in a line on each side.

In this study, A36 mild steel was used as the tube material. This material has the following parameters (Lacy, 2010): initial yield $a = 146.7$ MPa, strain hardening $b = 896.9$ MPa, strain hardening exponent $n = 0.320$, strain rate coefficient $c = 0.033$, thermal softening $M = 0.323$, reference strain rate $\dot{\varepsilon}_0 = 1.0$ s⁻¹, Young's modulus $E = 200$ GPa, and density $\rho = 7850$ kg/m³. A nonlinear finite element code, ABAQUS-Explicit, was used to establish finite element models of square steel tubes. Homogeneous continuum shells with five integration points in the thickness direction of the element

TABLE 2 Design of experiment according to face-centered CCD.

Run	Height, A (mm)	Width, B (mm)	Distance, C (mm)	PF (kN)		MCF (kN)		CFE		SEA (kJ/kg)	
				Actual	Predicted	Actual	Predicted	Actual	Predicted	Actual	Predicted
1	10	22.5	27.5	224.17	224.15	119.93	119.94	0.535	0.535	14.53	14.53
2	10	43.5224	27.5	198.88	199.17	111.10	111.51	0.559	0.559	13.68	13.63
3	5	10	15	216.19	212.68	111.44	112.02	0.515	0.524	13.62	13.61
4	15	10	40	221.05	226.48	117.89	117.48	0.533	0.519	14.25	14.17
5	1.59104	22.5	27.5	219.37	224.52	115.01	114.19	0.524	0.506	13.93	13.89
6	10	22.5	48.5224	220.81	215.32	119.61	119.97	0.542	0.558	14.50	14.53
7	5	35	15	206.35	200.25	101.32	101.83	0.491	0.514	12.41	12.48
8	10	22.5	27.5	224.17	224.15	119.93	119.94	0.535	0.535	14.53	14.53
9	15	35	15	185.43	186	108.32	107.87	0.584	0.583	13.13	13.12
10	10	22.5	27.5	224.17	224.15	119.93	119.94	0.535	0.535	14.53	14.53
11	10	22.5	27.5	224.17	224.15	119.93	119.94	0.535	0.535	14.53	14.53
12	15	35	40	212.00	214.84	119.36	118.88	0.563	0.551	14.45	14.46
13	18.409	22.5	27.5	225.01	220.79	116.76	117.43	0.519	0.533	14.18	14.23
14	5	10	40	217.92	216.68	119.10	119.66	0.547	0.556	14.40	14.41
15	10	22.5	6.47759	181.30	187.71	104.78	104.28	0.578	0.558	12.76	12.73
16	15	10	15	212.00	209.69	115.50	115.79	0.545	0.551	14.07	14.07
17	10	22.5	27.5	224.17	224.15	119.93	119.94	0.535	0.535	14.53	14.53
18	5	35	40	214.65	216.3	119.00	118.8	0.554	0.546	14.51	14.51
19	10	22.5	27.5	224.17	224.15	119.93	119.94	0.535	0.535	14.53	14.53
20	10	1.47759	27.5	218.77	219.41	119.46	118.9	0.546	0.541	14.29	14.34

were employed to model the square-tube structure. A 5-mm-sized mesh consistent with the square-tube model without a crush initiator, was used. A general contact-component interaction model was employed to simulate the contact between two or more surfaces in contact or adjacent to each other. General contact models are widely used in crash simulations, structural dynamics analyses, and manufacturing process simulations. The contact between the impactor and square tube was modeled as a finite sliding penalty with a Coulomb friction coefficient of 0.2 (Altin et al., 2017). A tie constraint was applied to prevent any relative movements between the square tube and fixed base, serving as an interaction between the two components.

3 Results and discussion

3.1 Development and verification of RSM model

Four different responses were analyzed in this study: PF, MCF, CFE, and SEA. These responses were analyzed by varying the height, width, and center distance of an elliptical crush initiator at the top end of a square steel tube. The experiment was conducted

using a face-centered CCD for each input parameter. The results are presented in Table 2. Design-Expert software (Anderson and Whitcomb, 2017) was employed to determine the square regression coefficients (R^2) of the developed model, perform regression fitting, and conduct the response surface study (Kallath et al., 2021). The square regression coefficients (R^2) of the PF, MCF, CFE, and SEA were 0.9308, 0.9939, 0.7200, and 0.9975, respectively. The quadratic-order models developed to represent crashworthiness performance were good, as evidenced by the high R^2 values for each indicator, which were close to 1.

Table 3 lists the ANOVA values for all responses and the suggested model for each response, which involves a quadratic order process to calculate the sum of squares, F-values, and p-values for each input parameter, their squares, and interactions. This table lists data on the sum of the squares of the model, residuals, and lack of fit for each response. Based on the data, the PF model is statistically significant, with an F-value of 14.95 and a corresponding p-value <0.05, indicating its sensitivity to any changes occurring in the input. The PF model is expressed by Eq. 9.

$$PF = 224.15 - 1.11A - 6.02B + 8.21C - 2.81AB + 3.2AC + 3.01BC$$
$$- 0.5263A^2 - 5.25B^2 - 8C^2 \tag{9}$$

TABLE 3 ANOVA results for all responses.

Response	Process order	Source	Sum of squares	Degree of freedom	Mean square	F-value	p-value
PF	Quadratic	Model	2,867.82	9	318.65	14.95	0.0001
		Residual	213.1	10	21.31		
		Lack of Fit	213.1	5	42.62		
MCF	Quadratic	Model	594.36	9	66.04	182.39	<0.0001
		Residual	3.62	10	0.3621		
		Lack of Fit	3.62	5	0.7242		
CFE	Quadratic	Model	0.0061	8	0.0008	3.54	0.0281
		Residual	0.0024	11	0.0002		
		Lack of Fit	0.0024	6	0.0004		
SEA	Quadratic	Model	7.69	9	0.8547	434.93	<0.0001
		Residual	0.0197	10	0.002		
		Lack of Fit	0.0197	5	0.0039		

The statistical analysis of the MCF model reveals an F-value of 182.39 and a corresponding p-value <0.05, indicating that the model is highly sensitive to changes in the input. The MCF model is expressed by Eq. 10.

$$MCF = 119.94 + 0.9632A - 2.2B + 4.66C + 0.5647AB - 1.49AC$$
$$+ 2.33BC - 1.46A^2 - 1.67B^2 - 2.76C^2$$

$$(10)$$

The CFE model had an F-value of 3.54 and a corresponding p-value <0.05, indicating sensitive to changes in the input. The CFE model can be expressed by Eq. 11.

$$CFE = 0.5351 + 0.008A + 0.0054B + 0.0001C + 0.0107AB$$
$$- 0.0159AC - 0.0055A^2 + 0.0054B^2 + 0.008C^2 \quad (11)$$

Statistical analysis of the SEA model revealed an F-value of 434.93 and a corresponding p-value <0.05, indicating that the model is highly significant and sensitive to changes in the input. The SEA model can be expressed by Eq. 12.

$$SEA = 14.53 + 0.1016A - 0.2106B + 0.5344C + 0.0469AB$$
$$- 0.1730AC + 0.3080BC - 0.1666A^2 - 0.1913B^2$$
$$- 0.3166C^2 \quad (12)$$

Figure 7 shows the importance of each input parameter, square, and interaction for all the four responses. The results indicate that in the case of the PF, input parameter C^2 was the most significant, whereas A^2 was the least significant $(C^2 > C > B > B^2 > AC > BC > AB > A > A^2)$. In the case of the MCF, input parameter C was the most significant, whereas AB was the least significant $(C > C^2 > B > BC > B^2 > A^2 > AC > A > AB)$. In the case of CFE, input parameter AC was the most significant, whereas BC was the least significant $(AC > A = AB = C^2 > B = A^2 = B^2 > C > BC)$. In the case of the SEA, input parameter C was the most significant, whereas AB was the least significant $(C > C^2 > BC > B > B^2 > A^2 > AC > A > AB)$. These findings are consistent with those of Huang et al. (2010), indicating that the
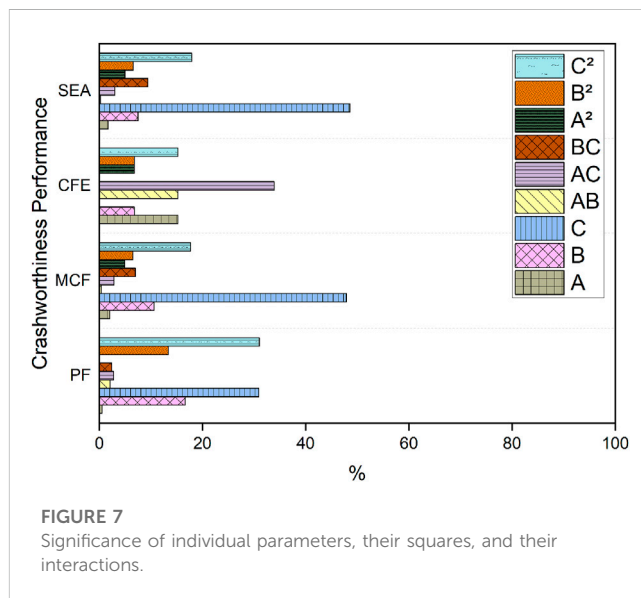

FIGURE 7
Significance of individual parameters, their squares, and their interactions.

position of the elliptical cut-out plays a crucial role in determining the SEA and reducing the PF. Moreover, it is considered optimal when the cut-out is closest to the impact source. Rogala et al. (2021b) reported that when the cut-out was placed at the same location, the cut-out width played a more significant role in decreasing the PF and increasing the SEA than the height. This study confirms the above findings regarding this statement. However, contrasting findings were obtained by Dadrasi et al. (2020), in which the height of the elliptical cutout had a more significant influence than its width. This discrepancy may be attributed to the fact that they only placed a single cutout on one side of the tube, whereas in this study, the cutout was positioned on all four sides of the square tube. Moreover, they adopted a rectangular cross-section, which could potentially lead to distinct crashworthiness behavior. Hence, further analysis of these variations should be conducted in future studies.
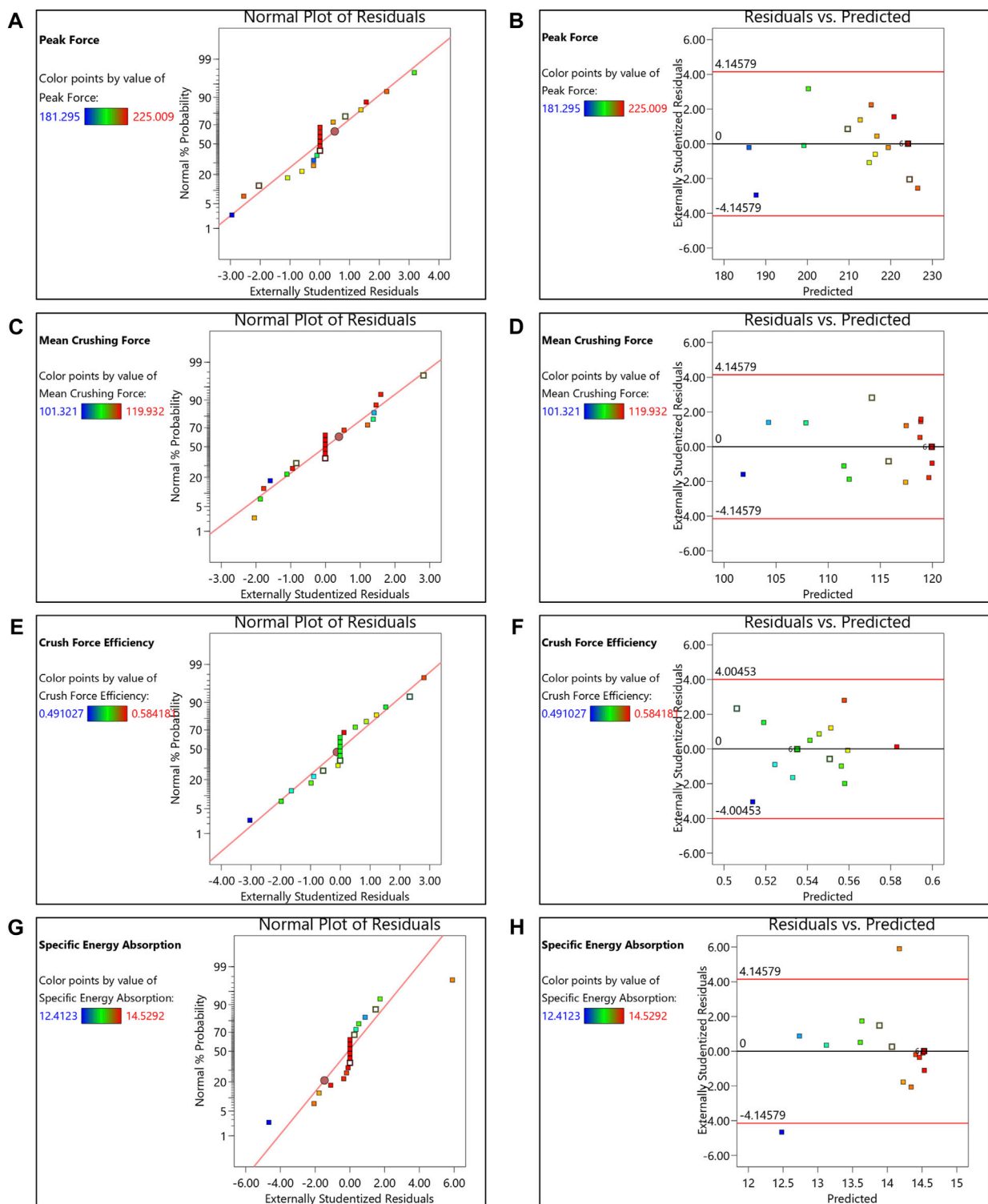
FIGURE 8
Normal plots of **(A)** residuals and **(B)** residuals-predicted for PF; normal plots of **(C)** residuals and **(D)** residuals-predicted for MCF; normal plots of **(E)** residuals and **(F)** residuals-predicted for CFE; normal plots of **(G)** residuals and **(H)** residuals-predicted for SEA.

The suitability and abnormality of data from the developed model were assessed using several normal plots of the residuals and residual-predicted plots (Anderson and Whitcomb, 2007). A model must have a good fit with the numerical data to be deemed acceptable, and the difference between the predicted and actual values should be minimal and follow a linear trend (Sahoo, 2011;
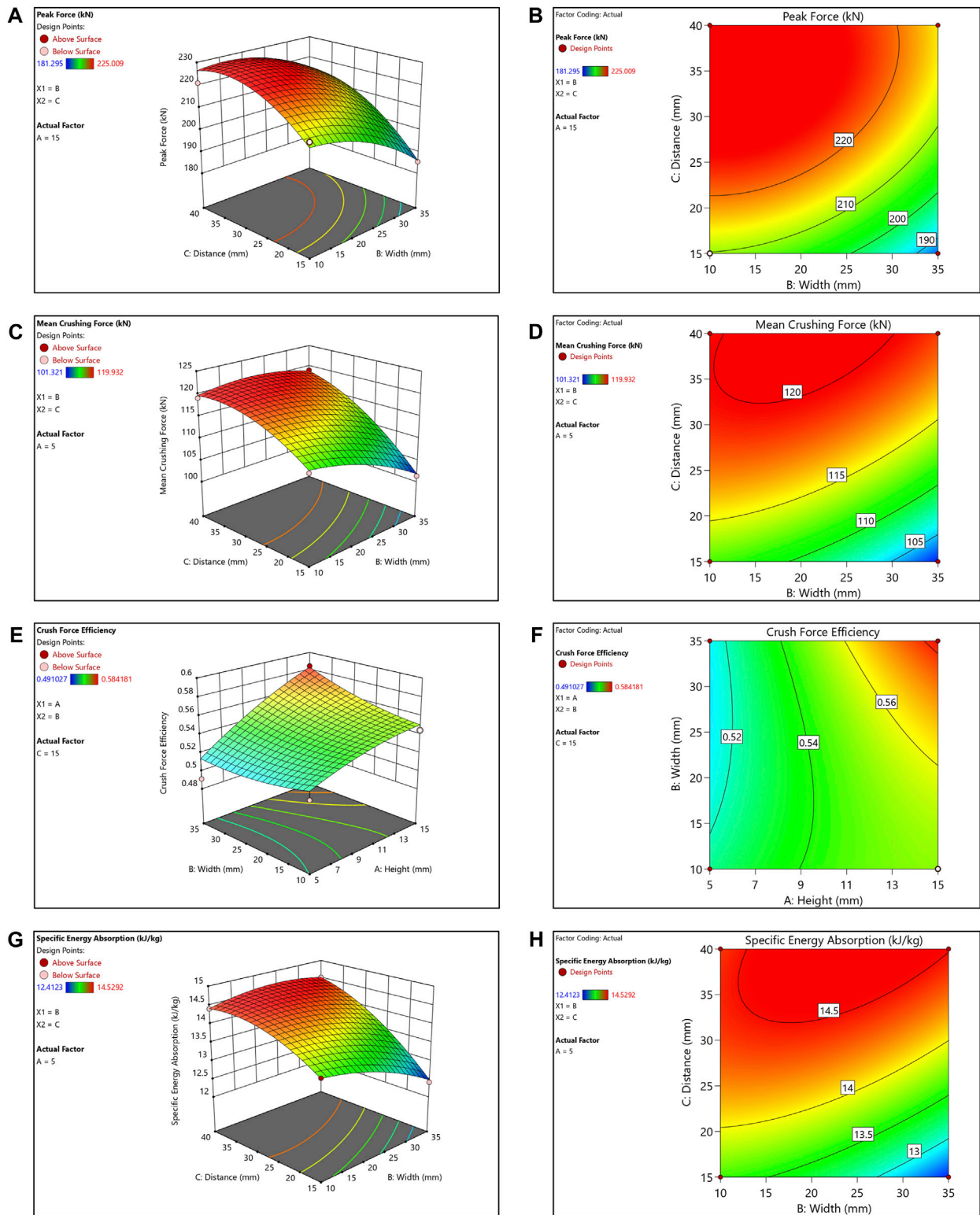
FIGURE 9
(A) 3-D surface and **(B)** contour of PF; **(C)** 3-D surface and **(D)** contour of MCF; **(E)** 3-D surface and **(F)** contour of CFE; **(G)** 3-D surface and **(H)** contour of SEA.

Deshwal et al., 2020; Maqsood et al., 2022), indicating a normal distribution of errors (Chakule et al., 2017). The residual and outlier plots for the PF, MCF, CFE, and SEA models are shown in Figure 8.

The data points on the normal plot of the residuals are randomly distributed and do not follow any particular pattern, indicating that the predictions by the proposed model are reliable. All data points in
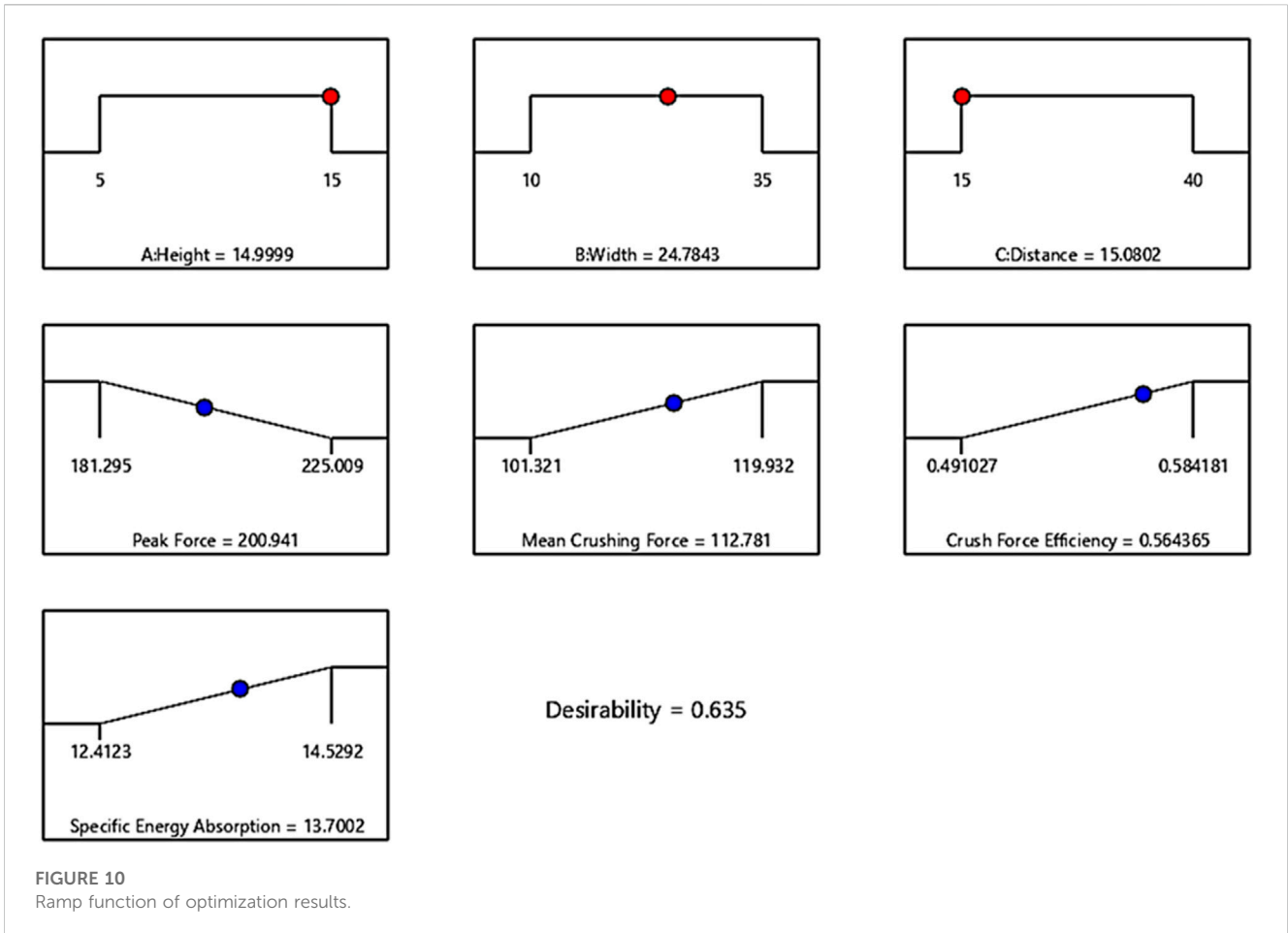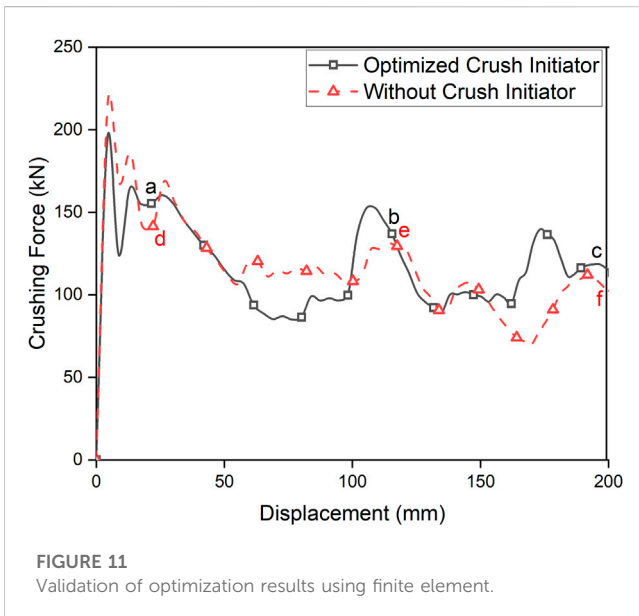
FIGURE 10
Ramp function of optimization results.

FIGURE 11
Validation of optimization results using finite element.

CFE ranged from +4.00453 to −4.00453. Despite the presence of a few outliers, the model demonstrated its ability to precisely capture the relationship between the input and response variables with a high R^2 value, even when dealing with noticeably different data points (Hawkins, 2004).

3.2 3-D surface predictive plots

This model has been analyzed and verified, and can help explore the design space. The 3-D surfaces comprehensively represent the responses when the input parameters are altered. Figure 9 shows the results of the numerical simulations and the use of 3-D surfaces and contours to depict the overall response using an RSM. One of the three input variables was kept constant at specific points, because displaying the interaction between more than two variables in a 3-D plot and contour was challenging. The selection of the constant variable was determined based on Figure 7, considering the linear coefficients that exhibited the lowest significance levels. Subsequently, the data points selected for the constant variable generated the highest or lowest values for each response.

Figures 9A,C,G show visual representations of the width (B) along the x-axis, distance (C) along the y-axis, and responses of the PF, MCF, and SEA along the z-axis. The height variable (A) remained constant because it was considered less significant than the other two input variables in the RSM model. Figure 9A is a 3-

the residual-predicted plot for the entire response model fell within an acceptable range, indicating the absence of outliers, except for two data points related to SEA. The acceptable values for the PF, MCF, and SEA ranged from +4.14579 to −4.14579, whereas those for the
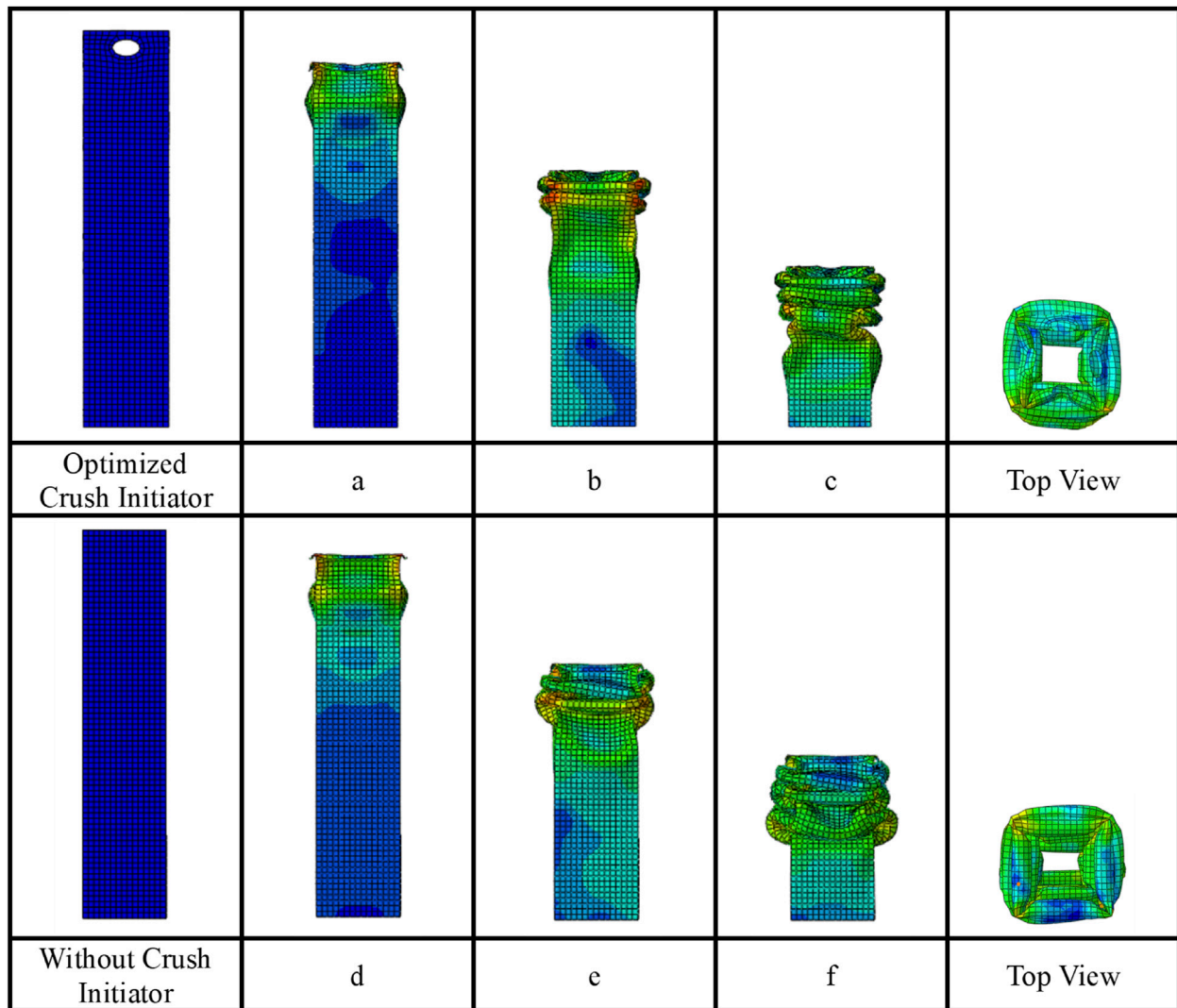
FIGURE 12
Collapse profile of square tube with optimized crush initiator and without crush initiator.

D surface graph with the height (*A*) fixed at 15 mm to highlight the range of PF values observed at that point in the data. When the crush initiator was closer to the top of the tube and wider, the PF values decreased. The influence of the height of the crush initiator became more significant as it increased. Figures 9C,G show 3-D surface graphs with the height (*A*) set at 5 mm to demonstrate the range of the MCF and SEA values observed at that specific data point. The MCF values increased when the crush initiator was farther from the top of the tube, and its width was narrower. However, when the MCF values were low at distances very close to the impact source, this can be compensated for by increasing the height of the crush initiator, yielding MCF values even higher than those observed in a tube without a crush initiator. For the SEA response, the values increased with increasing distance of the crush initiator from the top of the tube. When the crush initiator was positioned near the impact source, a reduction in the SEA occurred simultaneously with an

increase in the width of the crush initiator. Conversely, when the crush initiator was far from the impact source, the SEA increased with the crush initiator width. Increasing the height of the crush initiator improves the SEA when it is positioned as close as possible to the impact source, but reduces it when the crush initiator is far from the impact source.

Figure 9E shows the height (*A*) along the *x*-axis, width (*B*) along the *y*-axis, and the CFE response along the *z*-axis. The distance (*C*) variable was kept constant because it was less significant than the other two input variables in the RSM model. The distance (*C*) was set at 15 mm to obtain the maximum and minimum values of the CFE at that specific data point using a 3-D surface graph. Longer heights and widths resulted in higher CFE values for crush initiators located close to the impact source. However, for the crush initiators positioned near the impact source, decreasing the width and increasing the height of the crush initiator decreased the CFE. When the crush initiator is far from the impact source and has

an extended width, the influence of the height can be disregarded in the changes to the CFE value.

Consequently, designing an elliptical cut-out as a crush initiator in square steel tubes is a complex task because enhancing one crashworthiness performance indicator may compromise another. Hence, the optimization process is crucial for attaining an energy absorber that exhibits the highest performance across all crashworthiness indicators.

3.3 Optimization results

Designing an energy-absorbing tube with a square steel shape and crushing it to achieve a high CFE while maintaining an SEA is challenging. The design process must reflect all the crashworthiness performance indices. Typically, the design of an energy absorber aims to minimize the PF and maximize the MCF, CFE, and SEA. These input parameters are set within a specified range to achieve various optimization objectives (Djamaluddin, 2023). The weights and importance factors for all responses were uniform because all crashworthiness performance indicators were regarded as equal in this design. Eq. 13 expresses the expression for multiobjective optimization.

$$\begin{cases} \text{Min } PF \\ \text{Max } MCF \\ \text{Max } CFE \\ \text{Max } SEA \\ \text{subject to} \quad 5 \le A \le 15 \\ \qquad\qquad\quad 10 \le B \le 35 \\ \qquad\qquad\quad 15 \le C \le 40 \end{cases} \qquad (13)$$

Figure 10 shows the ramp function of the optimization results. By employing an RSM for the optimization, optimal outcomes for the dimensions and positions of the elliptical crush initiator were obtained, with a height of 15 mm, width of 24.784 mm, and distance of 15.08 mm. The optimum values corresponding to these points for the PF, MCF, CFE, and SEA were 200.94 kN, 112.78 kN, 0.564, and 13.70 kJ/kg, respectively. The optimization results revealed an overall desirability (D) of 0.635, which served as a metric to gauge how closely a combination of input parameters approached the desired response in the design of an elliptical crush initiator. Desirability scores range from 0 to 1, with a score of 1 indicating that the obtained response matches the desired optimum value (Anderson and Whitcomb, 2017). The optimization results demonstrated that CFE obtained the highest desirability score, whereas PF achieved the lowest score ($d_{CFE} > d_{MCF} > d_{SEA} > d_{PF}$). It should be noted that desirability does not affect the quality of the optimization process, as the main objective is to obtain responses that align with the optimization objectives, rather than to achieve a desirability score of 1.

The dimensions and positions of the optimized elliptical crush initiator were verified through finite element simulations, as shown in Figure 11. Figure 12 shows the deformation patterns that matched the selected points during the impact test. The highest error between the optimization outcome using the RSM and that employing the finite element method was 4.8% for the CFE. This level of disparity is deemed acceptable.

The finite element simulation results for the PF, MCF, CFE, and SEA obtained using the optimized dimensions and position of an elliptical cut-out were 195.06 kN, 115.3 kN, 0.591, and 13.89 kJ/kg, respectively. Based on finite element simulations, it was found that the optimal incorporation of crush initiators determined using the RSM resulted in a 10.12% decrease in PF, a 13.67% increase in CFE, and a 2.23% increase in MCF. However, these outcomes were offset by a slight decrease of 0.82% in the SEA.

4 Conclusion

This study focuses on the numerical analysis of how the dimensions and distance of an elliptical crush initiator positioned at the top end of a square tube influence its crashworthiness performance. The RSM was used in this study to predict the outcomes and evaluate the impacts of the geometric inputs on the PF, MCF, CFE, and SEA. The experiment involved selecting three input parameters and employing a face-centered CCD to observe their effects on the various responses. The RSM approach favors a quadratic process order. Based on the results of this study, several conclusions can be drawn. Various input parameters have varying significances for different responses. The squared distance input parameter most significantly impacted PF, and the distance input parameter had the greatest influence on the MCF. The interaction between height and distance influences the CFE, and the distance input parameter significantly influences the SEA.

The RSM optimization process yielded an optimal elliptical crush initiator geometry with a height of 15 mm, width of 24.784 mm, and distance of 15.08 mm from the top end. The results were validated using finite element analysis. Based on these data points, the optimal values for PF, MCF, CFE, and SEA were determined as 195.06 kN, 115.3 kN, 0.591, and 13.89 kJ/kg, respectively, consistent with the collected data. The findings of this study are consistent with this objective, except for a slight decrease in SEA. This finding suggests that the optimized elliptical crush initiator effectively enhances the crashworthiness performance while preserving the SEA. Therefore, RSM has been successfully applied to determine the dimensions and positioning of elliptical crush initiators in thin-walled square-tube structures. Hence, future research can focus on detailed analysis of the variations in geometrical inputs observed in this study by incorporating additional modifications to the cross-sectional profile of the tube and the number of elliptical cutouts. This possibility has been previously mentioned and provides opportunities for further investigation.

Data availability statement

The original contributions presented in the study are included in the article/Supplementary Material, further inquiries can be directed to the corresponding author.

Author contributions

MH: Conceptualization, Methodology, Software, Validation, Visualization, Writing–original draft, Writing–review and editing. JI: Conceptualization, Funding acquisition, Methodology,

Supervision, Writing–review and editing. NN: Methodology, Software, Visualization, Writing–review and editing.

Funding

Acknowledgments

Conflict of interest

The authors declare that the research was conducted in the absence of any commercial or financial relationships that could be construed as a potential conflict of interest.

Publisher's note

All claims expressed in this article are solely those of the authors and do not necessarily represent those of their affiliated organizations, or those of the publisher, the editors and the reviewers. Any product that may be evaluated in this article, or claim that may be made by its manufacturer, is not guaranteed or endorsed by the publisher.

Supplementary material

The Supplementary Material for this article can be found online at: https://www.frontiersin.org/articles/10.3389/fmech.2023.1273447/full#supplementary-material

References

Abramowicz, W., and Jones, N. (1984). Dynamic axial crushing of square tubes. *Int. J. Impact Eng.* 2 (2), 179–208. doi:10.1016/0734-743X(84)90005-8

Altin, M., Güler, M. A., and Mert, S. K. (2017). The effect of percent foam fill ratio on the energy absorption capacity of axially compressed thin-walled multi-cell square and circular tubes. *Int. J. Mech. Sci.* 131, 368–379. doi:10.1016/j.ijmecsci.2017.07.003

Anderson, M. J., and Whitcomb, P. J. (2017). *DOE simplified: Practical tools for effective experimentation.* United States: CRC Press.

Anderson, M. J., and Whitcomb, P. J. (2007). Using graphical diagnostics to deal with bad data. *Qual. Eng.* 19 (2), 111–118. doi:10.1080/08982110701241434

Asanjarani, A., Mahdian, A., and Dibajian, S. H. (2018). Comparative analysis of energy absorption behavior of tapered and grooved thin-walled tubes with the various geometry of the cross section. *Mech. Adv. Mater. Struct.* 27 (8), 633–644. doi:10.1080/15376494.2018.1488311

Balaji, G., and Annamalai, K. (2017). An experimental and numerical scrutiny of crashworthiness variables for square column with V-notch and groove initiators under quasi-static loading. *Cogent Eng.* 4 (1). doi:10.1080/23311916.2017.1364118

Chakule, R. R., Chaudhari, S. S., and Talmale, P. (2017). Evaluation of the effects of machining parameters on MQL based surface grinding process using response surface methodology. *J. Mech. Sci. Technol.* 31 (8), 3907–3916. doi:10.1007/s12206-017-0736-6

Cheng, Q., Altenhof, W., and Li, L. (2006). Experimental investigations on the crush behaviour of AA6061-T6 aluminum square tubes with different types of through-hole discontinuities. *Thin-Walled Struct.* 44 (4), 441–454. doi:10.1016/j.tws.2006.03.017

Dadrasi, A., Albooyeh, A., Fooladpanjeh, S., Shad, M. D., and Beynaghi, M. (2020). RSM and ANN modeling of the energy absorption behavior of steel thin-walled columns: a multi-objective optimization using the genetic algorithm. *J. Braz. Soc. Mech. Sci. Eng.* 42 (11), 563. doi:10.1007/s40430-020-02643-5

Deshwal, S., Kumar, A., and Chhabra, D. (2020). Exercising hybrid statistical tools GA-RSM, GA-ANN and GA-ANFIS to optimize FDM process parameters for tensile strength improvement. *CIRP J. Manuf. Sci. Technol.* 31, 189–199. doi:10.1016/j.cirpj.2020.05.009

Dionisius, F., Istiyanto, J., Sumarsono, D. A., Prayogo, G., Baskoro, A. S., and Malawat, M. (2022). Modeling of crashworthiness criteria based on variation of hole as crush initiator in thin-walled square. *Int. J. Automot. Mech. Eng.* 19 (1), 9487–9497. doi:10.15282/ijame.19.1.2022.12.0731

Djamaluddin, F. (2023). Finite element analysis and optimization of foam filled fender under quasi static and dynamic responses. *Front. Mech. Eng.* 9, 1091345. doi:10.3389/fmech.2023.1091345

Estrada, Q., Szwedowicz, D., Rodriguez-Mendez, A., Elías-Espinosa, M., Silva-Aceves, J., Bedolla-Hernández, J., et al. (2019). Effect of radial clearance and holes as crush initiators on the crashworthiness performance of bi-tubular profiles. *Thin-Walled Struct.* 140, 43–59. doi:10.1016/j.tws.2019.02.039

Guler, M. A., Cerit, M. E., Bayram, B., Gerceker, B., and Karakaya, E. (2010). The effect of geometrical parameters on the energy absorption characteristics of thin-walled structures under axial impact loading. *Int. J. Crashworthiness* 15 (4), 377–390. doi:10.1080/13588260903488750

Hawkins, D. M. (2004). The problem of overfitting. *J. Chem. Inf. Comput. Sci.* 44 (1), 1–12. doi:10.1021/ci0342472

Huang, M. Y., Tai, Y. S., and Hu, H. T. (2010). Dynamic crushing characteristics of high strength steel cylinders with elliptical geometric discontinuities. *Theor. Appl. Fract. Mech.* 54 (1), 44–53. doi:10.1016/j.tafmec.2010.06.014

Kallath, H., Lee, J. S., Kholi, F. K., Ha, M. Y., and Min, J. K. (2021). A multi-objective airfoil shape optimization study using mesh morphing and response surface method. *J. Mech. Sci. Technol.* 35, 1075–1086. doi:10.1007/s12206-021-0221-0

Lacy, J. (2010). *Optimization-based constitutive parameter identification from Sparse Taylor cylinder data.* Idaho Falls, ID (United States): Idaho National Lab.

Li, Z., Rakheja, S., and Shangguan, W. B. (2019). Study on crushing behaviors of foam-filled thin-walled square tubes with different types and number of initiators under multiple angle loads. *Thin-Walled Struct.* 145. doi:10.1016/j.tws.2019.106376

Malawat, M., Sumarsono, D. A., Istiyanto, J., Prayogo, G., and Dionisius, F. (2019). Theoretical prediction of dynamic axial crushing on a square tube with eight holes used as a crush initiator. *Int. J. Technol.* 10 (5), 1042–1055. doi:10.14716/ijtech.v10i5.2297

Maqsood, K., Ali, A., Ilyas, S. U., Garg, S., Danish, M., Abdulrahman, A., et al. (2022). Multi-objective optimization of thermophysical properties of multiwalled carbon nanotubes based nanofluids. *Chemosphere* 286, 131690. doi:10.1016/j.chemosphere.2021.131690

Nagaraju, S., Vasantharaja, P., Chandrasekhar, N., Vasudevan, M., and Jayakumar, T. (2016). Optimization of welding process parameters for 9Cr-1Mo steel using RSM and GA. *Mater. Manuf. process.* 31 (3), 319–327. doi:10.1080/10426914.2015.1025974

Nghia, N. C., Dirgantara, T., Gunawan, L., Putra, I. S., and Anh, L. H. (2013). "Analytical prediction of square crash box structure with holes due to impact loading," in Proceeding of The Regional Conference on Mechanical and Manufacturing Engineering (RCMME), Kuala Lumpur, Malaysia, 25th November 2013.

Razazan, M., Rezvani, M. J., and Souzangarzadeh, H. (2018). Evaluation of the performance of initiator on energy absorption of foam-filled rectangular tubes: experimental and numerical assessment. *Exp. Tech.* 42 (2), 129–139. doi:10.1007/s40799-017-0206-1

Rezvani, M. J., and Jahan, A. (2015). Effect of initiator, design, and material on crashworthiness performance of thin-walled cylindrical tubes: A primary multi-criteria

analysis in lightweight design. *Thin-Walled Struct.* 96, 169–182. doi:10.1016/j.tws.2015.07.026

Rogala, M., Ferdynus, M., Gawdzińska, K., and Kochmański, P. (2021a). The influence of different length aluminum foam filling on mechanical behavior of a square thin-walled column. *Materials* 14 (13). doi:10.3390/ma14133630

Rogala, M., Gajewski, J., and Górecki, M. (2021b). Study on the effect of geometrical parameters of a hexagonal trigger on energy absorber performance using ann. *Materials* 14 (20). doi:10.3390/ma14205981

Sahoo, P. (2011). Optimization of turning parameters for surface roughness using RSM and GA. *Adv. Prod. Eng. Manag.* 6 (3), 197–208.

Subramaniyan, S. K., Kananasan, A. K., Yunus, M. R. M., Mahzan, S., and Ghazali, M. I. (2014). Crush characteristics and energy absorption of thin-walled tubes with through-hole crush initiators. *Appl. Mech. Mater.* 606, 181–185. doi:10.4028/www.scientific.net/AMM.606.181

Sun, G., Pang, T., Xu, C., Zheng, G., and Song, J. (2017). Energy absorption mechanics for variable thickness thin-walled structures. *Thin-Walled Struct.* 118, 214–228. doi:10.1016/j.tws.2017.04.004

Tarlochan, F., Samer, F., Hamouda, A. M. S., Ramesh, S., and Khalid, K. (2013). Design of thin wall structures for energy absorption applications: enhancement of crashworthiness due to axial and oblique impact forces. *Thin-Walled Struct.* 71, 7–17. doi:10.1016/j.tws.2013.04.003

Witteman, W. (1999). Improved vehicle crashworthiness design by control of the energy absorption for different collision situations. Eindhoven, Netherlands: University of Technology, Automotive Engineering and Product Design Technology. Ph. D. Thesis.